Spectrochimica Acta Part A: Molecular and Biomolecular Spectroscopy xxx (2014) xxx–xxx

Contents lists available at ScienceDirect

Spectrochimica Acta Part A: Molecular and Biomolecular Spectroscopy

journal homepage: www.elsevier.com/locate/saa

Ab-initio and DFT calculations on molecular structure, NBO, HOMO–LUMO study and a new vibrational analysis of 4-(Dimethylamino) Benzaldehyde

Mariana Rocha, Alejandro Di Santo, Juan Marcelo Arias, Diego M. Gil *, Aída Ben Altabef *,[1]

INQUINOA, CONICET, Instituto de Química Física, Facultad de Bioquímica, Química y Farmacia, Universidad Nacional de Tucumán, San Lorenzo 456, T4000CAN Tucumán, Argentina

HIGHLIGHTS

- The molecular structure 4-(Dimethylamino) Benzaldehyde has been optimized by ab initio and DFT methods.
- The vibrational frequencies and UV–visible spectrum have been calculated and correlated with the experimental data.
- NBO and AIM analysis were performed in order to evaluate the stability of the molecule.
- HOMO and LUMO analysis were used to evaluate some molecular properties.
- DSC measurements were performed to evaluate the thermodynamic parameters associated to different transitions.

GRAPHICAL ABSTRACT

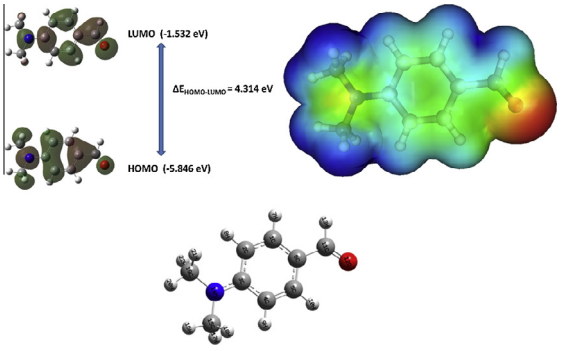

ARTICLE INFO

Article history:
Received 1 August 2014
Received in revised form 15 September 2014
Accepted 19 September 2014
Available online xxxx

Keywords:
DFT calculations
NBO analysis
AIM approach
IR and Raman spectroscopy
HOMO–LUMO analysis

ABSTRACT

The experimental and theoretical study on the molecular structure and a new vibrational analysis of 4-(Dimethylamino) Benzaldehyde (DMABA) is presented. The IR and Raman spectra were recorded in solid state. Optimized geometry, vibrational frequencies and various thermodynamic parameters of the title compound were calculated using DFT methods and are in agreement with the experimental values. A detailed interpretation of the IR and Raman spectra of the title compound were reported. The stability of the molecule arising from hyper-conjugative interactions and charge delocalization has been analyzed using NBO analysis and AIM approach. The HOMO and LUMO analysis were used to determine the charge transfer within the molecule and some molecular properties such as ionization potential, electron affinity, electronegativity, chemical potential, hardness, softness and global electrophilicity index. The TD-DFT approach was applied to assign the electronic transitions observed in the UV–visible spectrum measured experimentally. Molecular electrostatic potential map was performed by the DFT method. According to DSC measurements, the substance presents a melting point of 72.34 °C and decomposes at temperatures higher than 193 °C.

* Corresponding authors. Tel.: +54 381 4311044; fax: +54 381 4248169.
E-mail addresses: dmgil@fbqf.unt.edu.ar (D.M. Gil), altabef@fbqf.unt.edu.ar (A.B. Altabef).
[1] Member of the Research Career of CONICET.

http://dx.doi.org/10.1016/j.saa.2014.09.077
1386-1425/

Introduction

The compound 4-(Dimethylamino) Benzaldehyde (DMABA) was synthesized for the first time by Wu et al. [1]. This compound has a lot of applications because of it reacts with a great variety of molecular ionic species due to the availability of electron density provided by the amine group that could acts as an electron donor and an electron acceptor. DMABA is an important reagent for the determination of different substances such as indole [2], hydrazine [3] and amino-acids [4] by colorimetric methods of analysis and pyrrole derivates after derivatization with DMABA, also known as the Ehrlich's reagent [5]. Fritz et al. have reported that DMABA can be used as a reagent to develop latent fringermarks on paper surfaces yielding impressions that are both colored and photoluminescent [6]. According to the studies performed by Callender et al., the compound DMABA is converted to the corresponding alcohol in presence of nicotinamide adenine dinucleotide (NADH) and a catalytic amount of enzyme at neutral pH. The binding nature of the aromatic aldehyde to the catalytic site of liver alcohol dehydrogenase from horse (LADH) was studied using Raman spectroscopy [7].

In previous studies, the vibrational assignment of the IR and Raman spectra was performed in order to know the changes produced by complexation of the Zn cation with DMABA as ligand [8]. Kushto et al. have reported a normal coordinate analysis based on IR and Raman spectra of six isotopic forms of DMABA with the corresponding potential energy distribution [9]. In 2010, Ribeiro et al. have used an application of the combined spectroscopic and computational Pairs in Molecular Materials (PiMM) methodology to elucidate the crystal structure of DMABA [10]. This association of spectroscopic and computational results was a way to improve the contribution from vibrational spectroscopy to the elucidation of the crystal structures in complex systems [10]. In this study, we have observed some discrepancies in the assignment of some normal modes of vibrations compared with those reported by different authors, principally in the bands corresponding to the C(O)—H and $N(CH_3)_2$ vibrations.

In the present article the IR, Raman and UV–visible spectra have been recorded. These experimental measurements were complemented with quantum chemical calculations in order to obtain an optimized molecular structure. Differential Scanning Calorimetry (DSC) measurements were also carried out to evaluate the enthalpy (ΔH) and entropy (ΔS) variations associated with different transitions produced with the temperature increment. The barrier to internal rotation around the N—C bond has been calculated with DFT methods. The molecular geometry optimizations were performed using DFT and ab initio methods and different basis sets to assist the interpretation and assignment of experimental IR and Raman spectra. The geometrical parameters obtained by calculations were compared with those obtained by X-ray diffraction methods. The study was complemented with natural bond orbital (NBO) and Atoms in Molecules (AIM) analysis. The HOMO–LUMO analysis have been used to elucidate information regarding ionization potential (IP), electron affinity (EA), electronegativity (χ), electrophilicity index (ω), hardness (η), softness (S) and chemical potential (μ) and all correlated. UV–visible spectral analysis has also been used to elucidate the electronic transitions within the molecule in gas phase and in ethanol.

Experimental details

The compound under investigation namely DMABA is purchased from Sigma–Aldrich and it was used without further purification.

The FTIR spectrum of the compound in solid state was recorded at room temperature (RT) in KBr pellets in the 4000–400 cm^{-1} frequency range with a Perkin–Elmer GX1 Fourier Transform infrared instrument.

The Raman spectrum of the solid at RT was measured in the 3500–50 cm^{-1} interval with a Thermoscientific DXR Raman microscope. The Raman data were collected using a diode-pump, solid state laser of 532 nm (at 5 cm^{-1} spectral resolution), a con-focal aperture of 25 μm pinhole and 10× objective. The sample was placed on gold-coated sample slides. To achieve a sufficient signal to noise ratio, 30 spectral scans of 2 s each were accumulated during the measurements with the laser power maintained at 10 mW.

UV–visible measurements were recorded using quartz cells (10 mm optical path length) on a Beckman/DU 7500 spectrophotometer. For this purpose, a solution of 10^{-4} mol/L of DMABA in absolute ethanol was prepared. The spectrum was recorded between 800 and 200 nm.

Calorimetric measurements were performed using a differential scanning calorimeter Perkin Elmer Pyris DSC 6. The experiments were carried out using 3.980 mg of powdered sample sealed in aluminum pans with a mechanical crimp. Temperature and heat flow calibrations were made with standard samples of indium by using its melting transition. Enthalpy changes associated with the melting point of the sample in study (ΔH) were directly obtained from the DSC data by integrating the anomalous peak in the baseline subtracted curve. The entropy change relative to the phase transition was finally determined using the relationship $\Delta S = \Delta H/T$.

Computational details

Theoretical calculations were performed using the program package Gaussian 03 [11]. The potential energies associated with the C-N—C—C dihedral angle were calculated at B3LYP level using 6-31G(d,p) basis sets, with that torsion angle frozen and all other parameters allowed to relax. The total energy curves were sampled in steps of 10° using default convergence criteria as implemented in the Gaussian program [11]. Geometry optimizations were performed at the MP2 [12] and DFT levels using the 6-31G(d,p) basis sets. DFT calculations were performed using Becke's three-parameter hybrid exchange functional [13] (B3) combined with both the Lee–Yang–Parr gradient-corrected correlation functional [14] (LYP) and the same basis sets as for the MP2 calculations. The second DFT method used, mPW1PW91 [15] applies a modified Perdew–Wang exchange functional and Perdew–Wang 91 correlation functional [15]. All calculations were performed using standard gradient techniques and default convergence criteria. The stability of the optimized geometries was confirmed by wavenumber calculations, which gave positive values for all the obtained wavenumbers. The vibrational modes were assigned by means of visual inspection using the Gaussview 05 program [16]. A comparison was performed between the theoretically calculated frequencies and the experimentally measured frequencies. In this investigation we observed that the calculated frequencies were slightly greater than the fundamental frequencies.

The prediction of Raman intensities was carried out by following the procedure outlined below. The Raman activities (S_i) were calculated by Gaussian 03 and converted to relative Raman intensity (I_i) using the following relation from the basic theory of Raman scattering [17]:

$$I_i = \frac{f(v_o - v_i)^4 S_i}{v_i[1 - \exp(-hcv_i/kT)]} \quad (1)$$

where v_o is the laser exciting wavenumber in cm^{-1} (in this work, we have used the excitation wavenumber $v_o = 18796.9\ cm^{-1}$, which corresponds to the wavelength of 532 nm of the solid state laser), v_i the vibrational wavenumber of the ith normal mode (in cm^{-1}),

Please cite this article in press as: M. Rocha et al., Ab-initio and DFT calculations on molecular structure, NBO, HOMO–LUMO study and a new vibrational analysis of 4-(Dimethylamino) Benzaldehyde, Spectrochimica Acta Part A: Molecular and Biomolecular Spectroscopy (2014), http://dx.doi.org/10.1016/j.saa.2014.09.077

h, *c* and *k* are universal constants, and *f* is the suitably chosen common scaling factor for all the peaks intensities (10^{-12}).

A natural bond orbital (NBO) calculation was performed at the B3LYP/6-31G(d,p) level using the program NBO 3.1 [18] as implemented in Gaussian 03 package. This analysis were performed in order to understand various second order interactions between the filled orbitals of one subsystem and vacant orbitals of another subsystem, in order to have a measure of the intra-molecular delocalization of hyper-conjugation. In addition, an analysis of the reactivity of the compound was done within Bader's atoms in molecules theory (AIM) by using the AIM2000 code [19,20].

The molecular properties such as ionization potential, electronegativity, chemical potential, chemical hardness and softness have been deduced from HOMO–LUMO analysis employing B3LYP/6-31G(d,p) method. The electronic absorption spectra for the optimized structures were calculated in gas phase and with a single-electron approximation and the SCRF, Polarizable Continuum Model (PCM) approximation in ethanol with the time dependent DFT (TD-DFT) at B3LYP/6-31G(d,p) level of theory.

Results and discussion

Quantum chemical calculations

Molecular structure

The potential energy surface scans for internal rotation around C(4)—C(3)—N(14)—C(15) dihedral angle (Fig. S1) was calculated at B3LYP/6-31G(d,p) level in order to evaluate the minima energy structures adopted for the title compound. Two minima corresponding to equivalent structures with the same energy were obtained according to the position of the C(15)H_3 with respect to the C(3)═C(4) bond. In the structure labeled as I, the CH_3 group is *syn* respect to the C═C bond and in the structure II, the CH_3 group is *anti* respect to the C═C bond. Fig. 1 shows the optimized molecular structure of the title compound calculated at B3LYP/6-31G(d,p) level. The dihedral angles O(12)—C(11)—C(6)—C(1) and C(4)—C(3)—N(14)—C(19) are 180 and 179.9°, respectively indicating that in the molecule, the aldehyde and dimethylamino groups are essentially coplanar with the benzene ring. The optimized geometrical parameters calculated at different levels of theory are shown in Table 1. These results are compared with the structure determined by X-ray diffraction methods [21]. In the crystal structure reported by Gao et al. the compound crystallizes with two independent and identical molecules in the asymmetric unit. Both molecules are linked via C—H···π interactions [21]. The experimental and theoretical data show that the C—C bond lengths are observed in the range 1.375–1.422 Å. The other values show that our calculated results are consistent with the experimental data. As shown in Table 1, the bond distances calculated by electron correlated methods are longer than the experimental distances. This situation is clearly observed in the distances where hydrogen is present such as C—H distances. The C—C bond lengths calculated at mPW1PW91/6-31G(d,p) level reproduce better the experimental results, however the differences observed in bond angles calculated at B3LYP/6-31G(d,p) level are lower than other methods compared with the experimental data. The bond lengths and bond

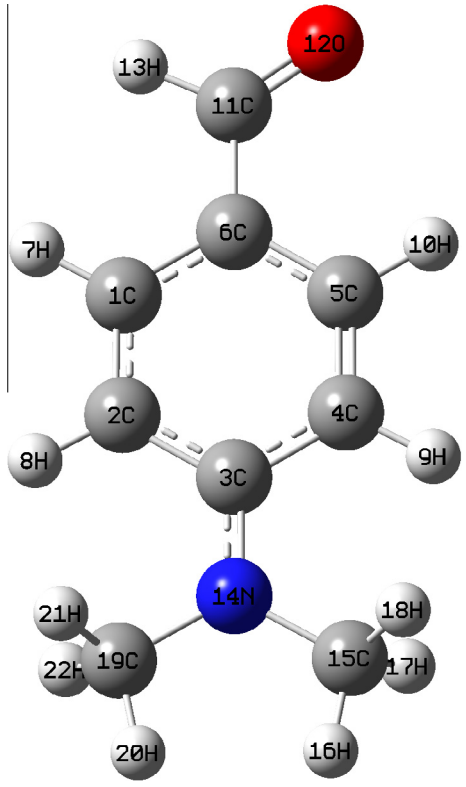

Fig. 1. Optimized molecular structure of DMABA calculated at B3LYP/6-31G(d,p) level of theory.

Table 1
Optimized geometrical parameters (bond lengths, angles and dihedral angles) for 4-(Dimethylamino) Benzaldehyde calculated at different levels of theory.

Parameters[a]	B3LYP	mPW1PW91	MP2	Experimental[b]
	6-31G(d,p)			
C(11)—H(13)	1.114	1.113	1.107	0.930
C(11)═O(12)	1.221	1.216	1.228	1.204
C(6)—C(11)	1.467	1.463	1.471	1.457
C(6)—C(1)	1.402	1.398	1.398	1.386
C(1)—C(2)	1.386	1.382	1.389	1.375
C(2)—C(3)	1.418	1.414	1.412	1.407
C(3)—C(4)	1.422	1.417	1.416	1.407
C(4)—C(5)	1.382	1.379	1.386	1.379
C(5)—C(6)	1.405	1.401	1.400	1.389
C(3)—N(14)	1.377	1.369	1.390	1.366
N(14)—C(15)	1.454	1.445	1.454	1.454
N(14)—C(19)	1.454	1.445	1.454	1.448
C(1)—H	1.088	1.087	1.085	0.930
C(2)—H	1.083	1.082	1.079	0.930
C(5)—H	1.086	1.085	1.083	0.930
C(4)—H	1.083	1.082	1.079	0.930
C(15)—H mean	1.095	1.094	1.090	0.960
C(19)—H mean	1.095	1.094	1.090	0.960
RMSD	0.0966	0.0958	0.0939	–
H—C(11)═O(12)	120.5	120.5	120.6	116.9
O(12)═C(11)—C(6)	125.2	125.1	124.6	126.2
C(11)—C(6)—C(5)	121.0	120.9	120.8	121.1
C(6)—C(5)—C(4)	121.2	121.2	120.7	121.0
C(5)—C(4)—C(3)	120.8	120.8	121.0	120.9
C(4)—C(3)—N(14)	121.1	121.0	121.0	120.9
C(3)—N(14)—C(15)	120.3	120.2	117.9	120.9
C(3)—N(14)—C(19)	120.2	120.1	117.8	121.1
C(3)—C(2)—C(1)	120.5	120.5	120.7	120.6
C(2)—C(1)—C(6)	121.5	121.4	120.9	121.7
C(1)—C(6)—C(11)	120.8	120.8	120.4	120.7
RMSD	1.1789	1.2011	1.8360	–
O(12)—C(1)—C(6)—C(5)	0.000	0.001	0.402	−1.60
C(11)—C(6)—C(5)—C(4)	180.0	179.9	179.8	−179.1
C(6)—C(5)—C(4)—C(3)	0.000	0.002	0.518	−0.800
C(5)—C(4)—C(3)—N(14)	179.9	179.9	177.9	−179.7
C(4)—C(3)—N(14)—C(15)	0.010	0.029	18.40	−4.700
C(4)—C(3)—N(14)—C(19)	179.9	179.9	165.2	179.4
N(14)—C(3)—C(2)—C(1)	−179.9	−179.9	−177.9	−179.6
C(3)—C(2)—C(1)—C(6)	0.000	0.001	0.431	−0.600
C(2)—C(1)—C(6)—C(11)	180.0	179.9	179.8	179.8
O(12)—C(11)—C(6)—C(1)	179.9	179.9	179.5	178.6

[a] Calculated with 6-31G(d,p) basis sets. See Fig. 1 for atoms numbering.
[b] Taken from Ref. [21].

Please cite this article in press as: M. Rocha et al., Ab-initio and DFT calculations on molecular structure, NBO, HOMO–LUMO study and a new vibrational analysis of 4-(Dimethylamino) Benzaldehyde, Spectrochimica Acta Part A: Molecular and Biomolecular Spectroscopy (2014), http://dx.doi.org/10.1016/j.saa.2014.09.077

angles comparisons were expressed in terms of root-mean-square deviations (RMSD) values and it reveal that the bond lengths have a better correlation (0.0939) using the MP2/6-31G(d,p) level of theory; however the bond angles have a better correlation (1.178) when we use the B3LYP method with the same basis sets.

The thermodynamic parameters of the title compound have also been computed. These calculations were performed in order to get reliable data from which the relations among energy, structure and reactivity characteristics of the molecule can be obtained. Knowledge of permanent dipole moment of a molecule provides wealth information. It can allow us to determine the molecular conformation of a substance. Table S1 indicates the value of some thermodynamic parameters (such as thermal energy, heat capacity, entropy, zero-point vibrational energies (ZPVEs), rotational constants and rotational temperatures) of DMABA calculated using only B3LYP/6-31G(d,p) level at 298.15 K. All the values are well agreed with the literature.

NBO analysis

NBO analysis has been performed on the DMABA molecule at B3LYP/6-31G(d,p) level of theory. Natural bond orbital (NBO) analysis is a useful tool for understanding delocalization of electron density from occupied Lewis-type (donor) NBOs to properly unoccupied non-Lewis type (acceptor) NBOs within the molecule. The stabilization of orbital interaction is proportional to the difference energy between the interacting orbitals. Therefore, the interaction having strongest stabilization takes place between effective donors and effective acceptors. The interaction between bonding and anti-bonding molecular orbitals can be quantitatively described in terms of NBO approach that is expressed by means of second-order perturbation interaction energy $E(2)$. This energy represents the estimate of the off-diagonal NBO Fock matrix element. The stabilization energy $E(2)$ associated with i (donor) $\rightarrow j$ (acceptor) delocalization is estimated from the second-order perturbation approach as given below [18]:

$$E(2) = \Delta E_{ij} = q_i \frac{F^2(i,j)}{\varepsilon_j - \varepsilon_i} \quad (2)$$

where q_i is the donor orbital occupancy, ε_i and ε_j are diagonal elements (orbital energies) and $F(i,j)$ is the off-diagonal Fock matrix element.

Table 2 shows the most relevant hyper-conjugative interactions for the title compound performed by NBO analysis. The hyper-conjugative interactions are formed by the orbital overlap between π (C—C) bond orbital to π* (C—C) anti-bonding orbital, which results in intra-molecular charge transfer causing the stabilization of the system. These interactions can be identified by finding the increase in electron density in the anti-bonding orbital. The strong inter-molecular hyper-conjugation interaction of the π electrons of C—C to anti C—C and C—O bond in the ring leads to stabilization of some part of the ring as can be shown in Table 2. Similar results were observed in 2-hydroxy-4-methoxy-acetophenone [22]. As can be seen in Table 2, the bond pair donor orbital π C—C → π* C—C and π C—C → π* C—O give more energy stabilization than σ C—C → σ* C—C. A very strong interaction has been observed between the lone electron pair LP N(14) and the σ* C(2)—C(3) with an energy of 47.67 kcal mol^{-1}. The lone pair LPO(2) only participates in LPO(2) → σ* C(6)—C(11) interaction with an important value of energy, as can be seen in Table 2. The energy value of the interactions π* C(2)—C(3) → π* C(1)—C(6) and π* C(2)—C(3) → π* C(4)—C(5) are 285.2 and 162.2 kcal mol^{-1}, respectively indicating that these interactions produce a great stabilization in the molecule.

Table 2
Second-order perturbation theory analysis of the Fock matrix for 4-(Dimethylamino) Benzaldehyde calculated by the NBO method.

Interaction (donor → acceptor)[a]	$E(2)$ kcal mol^{-1}[b]
π C(1)—C(6) → π* C(1)—C(6)	1.65
π C(1)—C(6) → π* C(2)—C(3)	16.17
π C(1)—C(6) → π* C(4)—C(5)	22.48
π C(1)—C(6) → π* C(11)—O(12)	23.51
π C(2)—C(3) → π* C(1)—C(6)	27.30
π C(2)—C(3) → π* C(2)—C(3)	1.13
π C(2)—C(3) → π* C(4)—C(5)	13.09
π C(4)—C(5) → π* C(1)—C(6)	14.19
π C(4)—C(5) → π* C(2)—C(3)	22.16
π C(11)—O(12) → π* C(1)—C(6)	4.79
π* C(2)—C(3) → π* C(1)—C(6)	285.22
π* C(2)—C(3) → π* C(4)—C(5)	162.15
π* C(11)—O(12) → π* C(4)—C(5)	0.75
σ C(1)—C(2) → σ* C(1)—C(6)	3.24
σ C(1)—C(2) → σ* C(2)—C(3)	3.15
σ C(1)—C(2) → σ* C(3)—N(14)	3.40
σ C(1)—C(2) → σ* C(6)—C(11)	3.11
σ C(1)—C(6) → σ* C(1)—C(2)	2.88
σ C(1)—C(6) → σ* C(5)—C(6)	3.80
σ C(1)—C(6) → σ* C(6)—C(11)	1.60
σ C(1)—C(6) → σ* C(11)—O(12)	1.44
σ C(2)—C(3) → σ* C(1)—C(2)	3.02
σ C(2)—C(3) → σ* C(3)—C(4)	3.42
σ C(2)—C0(3) → σ* C(3)—N(14)	1.71
σ C(2)—C(3) → σ* N(14)—C(15)	4.00
σ C(3)—C(4) → σ* C(2)—C(3)	3.43
σ C(3)—C(4) → σ* C(3)—N(14)	1.67
σ C(3)—C(4) → σ* C(4)—C(5)	2.97
σ C(3)—C(4) → σ* N(14)—C(19)	4.00
LPO(12) → σ* C(6)—C(11)	18.02
LPN(14) → σ* C(2)—C(3)	47.67

[a] See Fig. 1 for atoms numbering. LP denotes lone pair on the specified atom.
[b] $E(2)$ means energy of hyper-conjugative interactions.

AIM analysis

The quantum theory of atoms in molecules has been useful in the characterization of bonds through a topological analysis of the electronic charge density and their Laplacian at the Bond Critical Point (BCP) [19]. In the AIM theory the nature of the bonding interaction can be determined through an analysis of the properties of the charge density, ρ, and its Laplacian $\nabla^2(\rho)$ at the BCP, and through the properties of the atoms, which are obtained by integrating the charge density over the atom orbitals [19]. The molecular graph of the title compound using AIM program calculated at B3LYP/6-31G(d,p) level is presented in Fig. S2. Table 3 shows the bond critical point data for DMABA. As can be seen in Table 3, the value of charge density at the C(11)═O(12) bond critical point is larger and the Laplacian electron density is positive indicating that the electronic charge is depleted between the nuclei. The values of charge density for the C(11)—C(6), C(3)—N(14), N(14)—C(15) and N(14)—C(19) bond critical points are relatively high and the $\nabla^2(\rho)$ is negative. These results indicate that the charge density has been concentrated in the inter-nuclear region.

HOMO–LUMO analysis

The Highest occupied molecular orbital (HOMO) and the lowest un-occupied molecular orbital (LUMO) are very important parameters for quantum chemistry. These values help to exemplify the chemical reactivity and kinetic stability of the molecule. The HOMO represents the ability to donate an electron and the LUMO as electron acceptor represents the ability to obtain an electron. In order to evaluate the energetic behavior of the title compound, the HOMO–LUMO energy calculations were carried out by means B3LYP method using 6-31G(d,p) basis sets. The energies and the pictorial illustration of HOMO, LUMO, HOMO−1 and LUMO+1 fron-

Please cite this article in press as: M. Rocha et al., Ab-initio and DFT calculations on molecular structure, NBO, HOMO–LUMO study and a new vibrational analysis of 4-(Dimethylamino) Benzaldehyde, Spectrochimica Acta Part A: Molecular and Biomolecular Spectroscopy (2014), http://dx.doi.org/10.1016/j.saa.2014.09.077

Table 3
The B3LYP/6-31G(d,p) calculated Bond Critical Point (BCP) data and BCP distances (in a.u.) to attractors.

	X Y	X Y	X Y	X Y	X Y
	C(11)═O(12)	C(11)—C(6)	C(3)—N(14)	N(14)—C(15)	N(14)—C(19)
ρ	0.4004	0.2804	0.3112	0.2662	0.2666
∇^2	0.2512	−0.7196	−0.9312	−0.7692	−0.7712
BCP–X	0.7603	1.402	0.9333	1.681	1.679
BCP–Y	1.546	1.370	1.668	1.067	1.067
d (Å)	1.221	1.467	1.377	1.454	1.454
q (x)	0.292	0.2928	0.3556	−0.5059	−0.5059
q (y)	−0.4390	0.0576	−0.5059	0.1938	0.1924

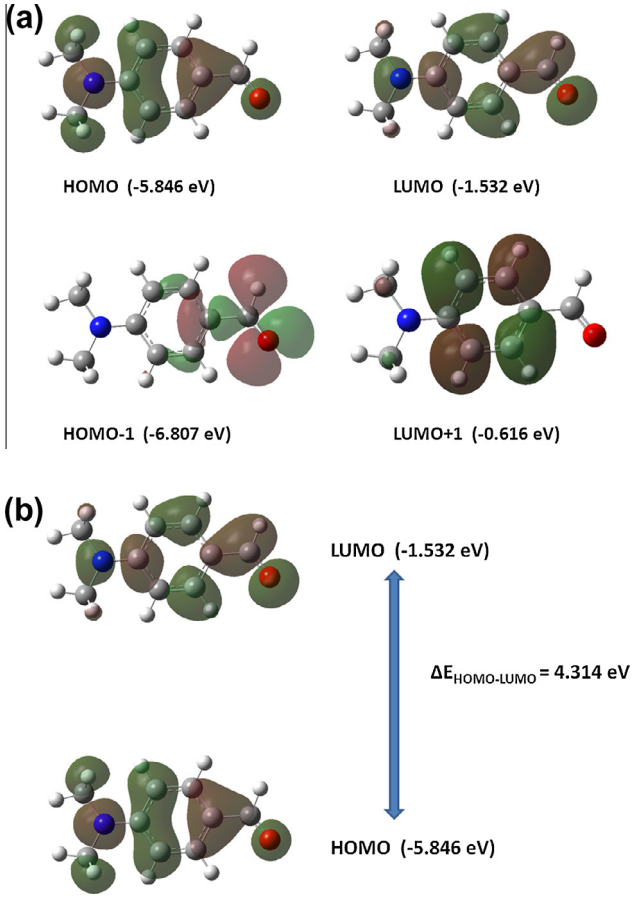

Fig. 2. (a) Frontier molecular orbitals (HOMO, LUMO, HOMO−1, LUMO+1) of DMABA calculated at B3LYP/6-31G(d,p) level. (b) HOMO and LUMO molecular orbitals and the $\Delta E_{HOMO-LUMO}$ energy gap for DMABA calculated at B3LYP/6-31G(d,p) level.

tier molecular orbitals are shown in Fig. 2(a). The positive and negative phase is represented in red and green color, respectively. The plots reveal that the HOMO is primarily composed of O(12), N(14), C(15) and C(19) of the methyl groups and C(6), C(2), C(3) and C(4) corresponding to the aromatic ring. The LUMO is spread over the entire molecule except on methyl groups bounded to N(14).

The energy gap ($E_{HOMO} - E_{LUMO}$) is an important value which serves as a stability index. In fact, a large HOMO–LUMO gap implies high molecular stability in the sense of its lower reactivity in chemical reactions [22,23]. The energy value of HOMO and LUMO molecular orbitals with the corresponding HOMO–LUMO energy gap is shown in Fig. 2(b). The HOMO–LUMO energy gap value is predicted to be 4.314 eV. This value explains the eventual charge transfer interaction with the molecule, which influences the biological activity of the compound. The relatively high value of $\Delta E_{HOMO-LUMO}$ indicates that the title compound presents high chemical stability and it has low reactivity.

Table 4
Frontier molecular orbital energies, HOMO–LUMO gap and global reactivity descriptors for DMABA calculated at B3LYP/6-31G(d,p) level.

Molecular parameters	B3LYP/6-31G(d,p)
E_{HOMO} (eV)	−5.846
E_{LUMO} (eV)	−1.532
$\Delta E_{HOMO-LUMO}$ (eV)	4.314
Ionization potential, IP (eV)	5.846
Electron affinity, EA (eV)	1.532
Electronegativity, χ (eV)	3.689
Chemical potential, μ (eV)	−3.689
Chemical hardness, η (eV)	2.157
Chemical softness, s (eV^{-1})	0.232
Global electrophilicity index, ω (eV)	3.154

In order to understand various aspects of pharmacological sciences including drug design and the possible eco-toxicological characteristics of the drug molecules, several new chemical reactivity descriptors have been proposed. Conceptual DFT based descriptors have helped in many ways to understand the structure of molecules and their reactivity by calculating the chemical potential, global hardness and electrophilicity. Using HOMO and LUMO orbital energies, the ionization potential (I) and electron affinity (A) can be expressed as: $I = -E_{HOMO}$ and $A = -E_{LUMO}$. Using these values we can calculate other chemical descriptors such as electronegativity $\chi = I + A/2$, chemical potential $\mu = -\chi$, hardness $\eta = I - A/2$, softness $s = 1/2\eta$ and global electrophilicity index $\omega = \mu^2/2\eta$ [24]. The global electrophilicity index was proposed by Parr et al. [25] and it measures the stabilization in energy when the system acquires an additional electronic charge from the environment. Electrophilicity encompasses both the ability of an electrophile to acquire additional electronic charge and the resistance of the system to exchange electronic charge with the environment. It contains information about both electron transfer (chemical potential) and stability (hardness) and is the better descriptor of global chemical reactivity. The energy of the frontier molecular orbitals HOMO and LUMO, $\Delta E_{HOMO-LUMO}$, electronegativity, chemical potential, hardness, softness and global electrophilicity index for the title compound calculated al B3LYP/6-31G(d,p) level are listed in Table 4. As can be seen in Table 4, the chemical potential is negative indicating that the compound is stable and does not decompose spontaneously into its elements. The hardness signifies the resistance towards the deformation of electron cloud of chemical systems under small perturbations encountered during chemical process. Considering the chemical hardness, if a molecule has large HOMO–LUMO gap, it is a hard molecule or small HOMO–LUMO gap it is a soft molecule. One can also relate the stability of a molecule to hardness, which means that the molecule with least HOMO–LUMO gap means is more reactive. Soft systems are large and highly polarizable, while hard systems are relatively small and much less polarizable.

Please cite this article in press as: M. Rocha et al., Ab-initio and DFT calculations on molecular structure, NBO, HOMO–LUMO study and a new vibrational analysis of 4-(Dimethylamino) Benzaldehyde, Spectrochimica Acta Part A: Molecular and Biomolecular Spectroscopy (2014), http://dx.doi.org/10.1016/j.saa.2014.09.077

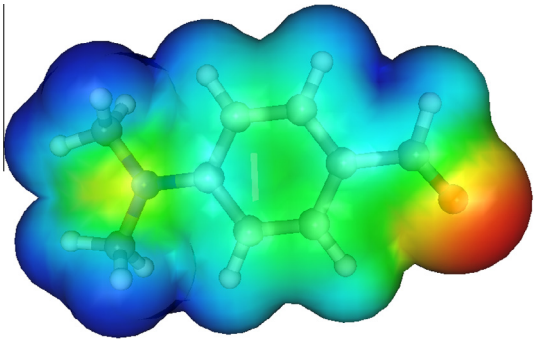

Fig. 3. Molecular electrostatic potential (MEP) plot for DMABA calculated by DFT methods.

Molecular electrostatic potential (MEP)

The molecular electrostatic potential (MEP) is related to the electron density and is a very useful descriptor in understanding sites for electrophilic and nucleophilic reactions as well as hydrogen bonding interactions [26,27]. To predict reactive sites of electrophilic or nucleophilic attacks for the investigated molecule, MEP at the B3LYP/6-31G(d,p) level optimized geometry was calculated. The different values of electrostatic potential at the MEP surface are represented by different colors: red, blue and green represent the regions of most negative, most positive and zero electrostatic potential, respectively. The negative electrostatic potential corresponds to an attraction of the proton by the aggregate electron density in the molecule (shades in red), while the positive electrostatic potential corresponds to a repulsion of the proton by the atomic nuclei (shade of blue). The negative (red and yellow) regions of MEP were related to electrophilic reactivity and the positive regions (blue) to nucleophilic reactivity. Fig. 3 shows the MEP plot for the title compound calculated by B3LYP method. From the MEP it is evident that the negative charge covers the C=O group and the positive region is over the hydrogen of the aromatic ring and over the hydrogen corresponding to the methyl groups. The value of the electrostatic potential is largely responsible for the binding of a substrate to its receptor binding sites since the receptor and the corresponding ligands recognize each other at their molecular surface [28,29].

UV–visible analysis

In order to understand the nature of electronic transitions within DMABA molecule, TD-DFT calculations on electronic absorption spectra in gas phase and in ethanol were performed. The λ_{max} values are obtained from the UV–visible spectra analyzed theoretically with B3LYP/6-31G(d,p) level of theory. The calculated UV absorption maxima, theoretical electronic excitation energies and oscillator strengths calculated in ethanol are detailed in Table 5. Table S2 shows the electronic excitation energies; wavelengths and oscillator strengths for the title compound calculated

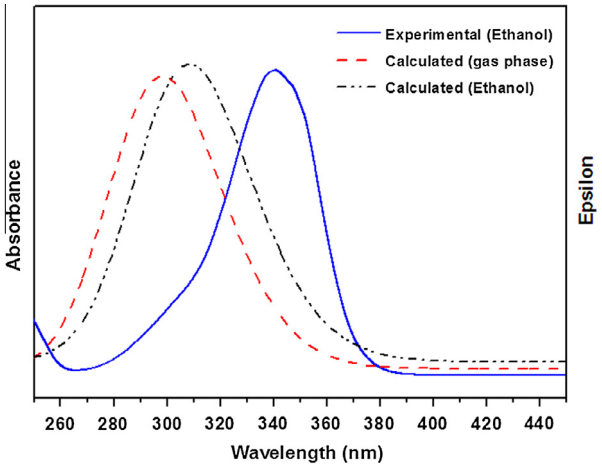

Fig. 4. Experimental and calculated UV–visible absorption spectra. The experimental spectrum was measured in 10^{-4} mol/L ethanol solutions. The calculated spectra in gas phase and in ethanol were calculated at B3LYP/6-31G(d,p) level.

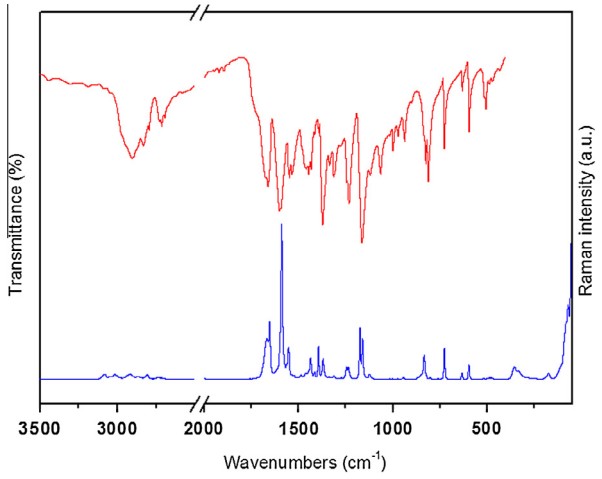

Fig. 5. Experimental IR and Raman spectra of DMABA in solid state.

in gas phase. The experimental and theoretical predicted UV–visible spectra are visualized in Fig. 4. As can be seen from Table 5, the calculated absorption maxima values for the title compound have been found to be 316, 309 and 272 nm. Oscillator strengths *f* is a dimensionless quantity that describes the strength of an electronic transition. Transitions with extremely low or zero *f* values are forbidden. The oscillator strength for the transition at 309 nm is higher in magnitude than the other transitions and its corresponding experimental value is observed at 340 nm. The maximum absorption at 340 nm is assigned to the transition from the HOMO to LUMO molecular orbital. This transition is predicted to be of $\pi \rightarrow \pi^*$ nature (see Fig. 2(b)). The absorption band located at

Table 5
Theoretical electronic absorption spectra of 4-(Dimethylamino) Benzaldehyde calculated at B3LYP/6-31G(d,p) level of theory.

Excited state	Wavelength (nm)		Excitation energies (eV)	Oscillator strengths (*f*)	Assignment
	Theoretical [a]	Experimental			
S1	316	–	3.928	0.0001	HOMO−1 → LUMO
S2	309	340	4.017	0.6172	HOMO → LUMO
S3	272	308	4.554	0.0229	HOMO → LUMO+1

[a] Calculated values in ethanol as solvent.

Please cite this article in press as: M. Rocha et al., Ab-initio and DFT calculations on molecular structure, NBO, HOMO–LUMO study and a new vibrational analysis of 4-(Dimethylamino) Benzaldehyde, Spectrochimica Acta Part A: Molecular and Biomolecular Spectroscopy (2014), http://dx.doi.org/10.1016/j.saa.2014.09.077

Table 6
Observed and calculated mode frequencies (in cm^{-1}) and tentative assignments for 4-(Dimethylamino) Benzaldehyde vibrations.

Mode	Experimental		Calculated [c]		Tentative assignment [d,e]
	IR [a]	Raman [b]	Unscaled	Scaled	
1	3104 sh	–	3230 (10)	3103	ν C(2)—H
2	3094 vw	–	32129(14)	3102	ν C(4)—H
3	–	3081 (3)	3204 (1)	3078	ν C(5)—H
4	3049 w	3052 (2)	3171 (12)	3047	ν C(1)—H
5	–	3020 (47)	3157 (35)	3033	ν_a CH_3
6	3012 vw	–	3145 (2)	3022	ν_a CH_3
7	–	2934 (3)	3061 (60)	2941	ν_a CH_3
8	–	2917 (3)	3059 (12)	2939	ν_a CH_3
9	2905 w	–	3017 (57)	2898	ν_s CH_3
10	2878 sh	2873 (2)	3009 (84)	2891	ν_s CH_3
11	2795 w	2809 (3)	2878 (170)	2765	ν C(11)—H
12	1661 s	1666 (26)	1782 (292)	1712	ν C=O
13	1594 vs	1589 (100)	1665 (478)	1599	ν C(4)—C(5) + ν C(1)—C(2)
14	1549 m	1553 (21)	1604 (48)	1541	ν C(1)—C(6) + ν C(2)—C(3)
15	1537 m	–	1573 (110)	1511	δ C—H
16	1485 w	1487 (2)	1545 (66)	1484	δ_a CH_3
17	1468 w	1467 (3)	1532 (4)	1472	δ_a CH_3
18	1446 w	1447 sh	1502 (13)	1443	δ_s CH_3
19	1432 w	1435 (14)	1502 (9)	1443	δ_a CH_3
20	1415 vw	1415 (5)	1493 (0)	1434	δ_a CH_3
21	1393 vw	1395 (21)	1485 (16)	1426	δ_s CH_3 + δ C—H
22	–	–	1458 (1)	1401	δ C—H + δ_s CH_3
23	1373 s	1370 (13)	1438 (6)	1382	δ C(11)—H
24	1336 w	1338 (2)	1401 (258)	1346	ν C(3)—N(14) + δ C—H
25	1314 m	1314 (2)	1383 (34)	1329	ν C(6)—C(5) + ν C(4)—C(3)
26	1245 w	1246 (8)	1345 (40)	1292	δ C—H
27	1233 m	1236 (8)	1283 (37)	1233	ν C(15)—N(14) + δ C—H
28	–	1174 (33)	1266 (47)	1216	ν C(6)—C(11) + δ C(11)—H + δ C—H
29	–	–	1203 (24)	1156	ν C(19)—N(14)
30	1166 vs	1161 (26)	1199 (179)	1152	δ C—H
31	1123 vw	1124 (3)	1154 (8)	1109	δ C—H
32	–	–	1151 (0)	1106	ρ CH_3
33	–	–	1141 (0)	1096	ρ CH_3
34	1065 vw	–	1086 (28)	1043	ρ CH_3
35	1001 vvw	1002 (<1)	1030 (0)	989	γ C(11)—H
36	–	–	1020 (3)	980	δ C(1)C(6)C(5) + δ C(2)C(3)C(4)
37	–	–	980 (0)	942	γ C—H
38	938 vw	942 (1)	968 (16)	930	ρ CH_3
39	–	–	952 (0)	915	γ C—H
40	833 vw	834 (15)	854 (22)	821	δ C=O + δ C(4)C(3)C(2)
41	825 w	824 sh	832 (44)	799	γ C—H + δ C(2)C(3)C(4)
42	813 m	810 (1)	817 (9)	785	γ C—H
43	729 m	727 (20)	742 (25)	713	δ C(2)C(1)C(6) + δ C=O
44	–	–	732 (0)	703	γ C(4)C(3)C(2) + γ C—H
45	633 w	634 (4)	659 (1)	633	δ C(2)C(1)C(6) + δ C(6)C(5)C(4)
46	596 m	597 (9)	611 (14)	587	δ C(19)N(14)C(15)
47	518 w	518 (1)	525 (6)	504	γ C(1)C(6)C(5) + γ C(4)C(3)C(2) + γ C—H
48	508 w	–	496 (3)	477	δ C(15)N(14)C(3)
49	492 vw	490 (1)	473 (5)	454	δ C(19)N(14)C(3)
50	472 vw	479 (1)	439 (<1)	422	γ C(2)C(1)C(6) + γ C(2)C(4)C(5)
51	–	357 (8)	343 (1)	329	δ C(1)C(6)C(11) + δ N(14)C(3)C(4)
52	–	335 (5)	341 (6)	328	γ C(19)N(19)C(15) + γ C(1)C(6)C(5)
53	–	247 (1)	272 (3)	261	δ C(11)C(6)C(5) + δ N(14)C(3)C(2)
54	–	–	241 (<1)	232	τ C(19)H_3
55	–	–	208 (<1)	199	τ C(15)H_3
56	–	–	167 (4)	160	τ Ring
57	–	177 (4)	164 (7)	158	τ C(11)—C(6) + τ C(19)H_3
58	–	–	88 (1)	85	τ CCCC
59	–	–	69 (1)	66	τ CCCC
60	–	–	40 (2)	38	τ N(14)—C(3)

[a] sh, shoulder; s, strong; w, weak; m, medium; v, very.
[b] Relative band heights in parentheses.
[c] Calculated at B3LYP/6-31G(d,p) level of theory. IR intensities are shown in parenthesis.
[d] ν: stretching, δ: in-plane deformation, γ: out-of-plane deformation, ρ: rocking, ω: wagging, τω: twisting, τ: torsion modes.
[e] See Fig. 1 for the atoms numbering scheme.

272 nm in the calculated spectrum (f = 0.0229) is assigned to the HOMO → LUMO+1 transition (n → π* nature). This band is observed experimentally as a shoulder located at 308 nm. The wavelength calculated at 316 nm (f = 0.0001) is mainly generated by excitations from the HOMO−1 to LUMO molecular orbital. This band was not observed experimentally.

Vibrational analysis

The 4-(Dimethylamino) Benzaldehyde molecule lacks of any symmetry (C_1 point group). Therefore, all 60 normal modes of vibrations are both IR and Raman active. The assignment of the observed bands in the solid state FTIR and Raman spectra of the

Please cite this article in press as: M. Rocha et al., Ab-initio and DFT calculations on molecular structure, NBO, HOMO–LUMO study and a new vibrational analysis of 4-(Dimethylamino) Benzaldehyde, Spectrochimica Acta Part A: Molecular and Biomolecular Spectroscopy (2014), http://dx.doi.org/10.1016/j.saa.2014.09.077

title compound was assisted by theoretical calculations. The frequencies were calculated in the harmonic approximation at the B3LYP/6-31G(d,p) level of theory. The experimental IR and Raman spectra are shown in Fig. 5. The simulated IR and Raman spectra of the title molecule are presented in Fig. S3. The experimental and calculated vibration frequencies are compared in Table 6 along a tentative mode assignment. The discrepancy observed between observed and calculated frequencies could be explained due to the fact that the inter-molecular interactions unavoidably present in the solid state is not taken into account in the gas phase theoretical calculations. Vibration mode frequencies calculated at B3LYP/6-31G(d,p) level were scaled by 0.9608 to correct for theoretical error in this work [30].

Assignment of bands

CH_3 vibrations. The anti-symmetric and symmetric stretching modes of the methyl groups generally appear at about 3100 and 2880 cm^{-1}. The bands observed at 3012 cm^{-1} in the IR spectrum and the bands at 3020, 2934 and 2917 cm^{-1} in Raman are assigned to the anti-symmetric stretching mode of the methyl group linked to the N atom. The bands located at 2905 and 2878 cm^{-1} in the IR spectrum (2873 cm^{-1} in Raman) are assigned to the methyl symmetric stretching vibration. Some discrepancies were observed with the assignment of the methyl modes reported by Rosencrance et al. in which the CH_3 stretching modes were reported in the range between 2912 and 2860 cm^{-1} [8].

The anti-symmetric methyl deformation modes are observed at 1485, 1468, 1432 and 1415 cm^{-1} in the IR spectrum and at 1487, 1467, 1435 and 1415 cm^{-1} in Raman. The IR bands located at 1446 and 1393 cm^{-1} are assigned to the symmetrical methyl deformation mode. The values reported in literature for these modes are expected in the range 1468–1371 cm^{-1} and the authors do not discriminate between symmetric and anti-symmetric bending modes of the methyl group [8]. The IR bands located at 1065 and 938 cm^{-1} are assigned to the rocking mode.

C—H vibrations. For all aromatic compounds, the C—H stretching vibrations are observed in the region 3100–3000 cm^{-1}. The bands located at 3104, 3094 and 3049 cm^{-1} in the IR spectrum (3081 and 3052 cm^{-1} in Raman) are assigned to the C—H stretching mode. These bands have been predicted at 3250–3170 cm^{-1} in calculations performed at B3LYP method. In aromatic compounds the C—H in-plane bending vibrations are observed in the region from 1300 to 850 cm^{-1} and are usually very weak. The bands due to the C—H in-plane ring vibrations coupled with C—C stretching vibrations are observed as a number of sharp medium to weak intensity bands in the 1400–1100 cm^{-1} spectral region. In the present study, the IR bands located at 1393, 1336, 1245, 1166 and 1123 cm^{-1} and the Raman bands at 1395, 1338, 1246, 1174, 1161 and 1124 cm^{-1} are assigned to the C—H in-plane bending mode as reported in Table 6. The C—H out-of-plane bending vibrations are strongly coupled vibrations and occur in the region from 950 to 600 cm^{-1} [30–35]. The IR bands observed at 825 and 813 cm^{-1} and the Raman bands located at 824 and 810 cm^{-1} confirm the presence of C—H out-of-plane bending vibrations, hence agreeing with the values predicted from calculations and reported in literature [30–35].

C—N, C—C and ring vibrations. The bands located at 1336 and 1233 cm^{-1} in the IR spectrum (1338 and 1236 cm^{-1} in Raman) are assigned to the C—N stretching vibrations. The frequency of these bands calculated at B3LYP method are 1401 and 1283 cm^{-1}, respectively. The C—N stretching vibrations reported by Rosencrance et al. are expected to be at 1155 and 937 cm^{-1} in the IR spectrum. These values are very different those reported previously [8].

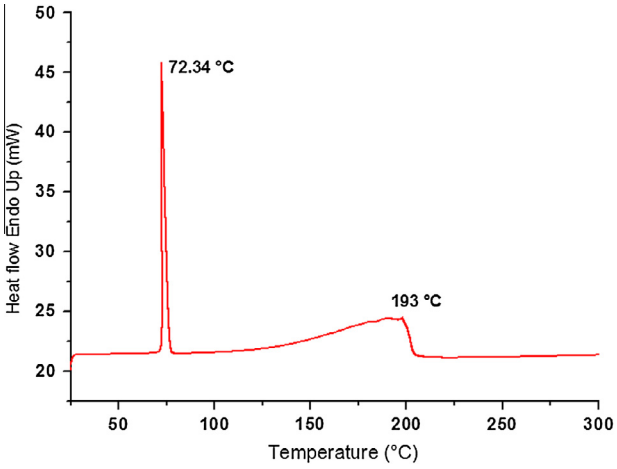

Fig. 6. DSC curve for solid state DMABA.

The phenyl group C—C stretching mode frequencies are expected in the spectral range from 1650 to 1200 cm^{-1}. The actual frequencies of these modes are determined not only by the nature of the substituents themselves but mainly by the way these are linked around the ring. The ring C—C stretching bands appear in the IR spectrum at 1594, 1549, 1314 cm^{-1} and at 1589, 1553 and 1314 cm^{-1} in Raman. The observed and calculated C—C—C in-plane and out-of-plane bending modes are presents in Table 6 along their assignment. These results are in good agreement with the corresponding literature data and provide support to values derived from theoretical calculations [30–35].

H—C=O vibrations. The C=O stretching vibration of the aldehyde groups give rise to bands at 1725 ± 65 cm^{-1} [36–37]. In this work, the C=O stretching mode of the title compound is observed at 1661 cm^{-1} in the IR spectrum and at 1666 cm^{-1} in Raman. The frequency calculated for the C=O stretching mode is 1782 cm^{-1}. An intense band located at 1676 cm^{-1} in both IR and Raman spectra has been attributed to the C=O stretching mode in Fermi resonance with the overtone of a ring mode that occurs at approximately 830 cm^{-1} [9].

The C—H stretching vibrations give rise to bands in the region 2830–2695 cm^{-1} in aldehyde groups [37]. The weak band located at 2795 cm^{-1} in the IR spectrum (2809 cm^{-1} in Raman) is assigned to the C(O)—H stretching mode. This band has been predicted at 2878 cm^{-1} by calculations. The C(O)—H stretching vibration reported by Ribeiro et al. was 2773 cm^{-1}, a very different value that those obtained in our work [10].

Differential Scanning Calorimetry (DSC) study

The aim of the present DSC study was to examine the possible structural transitions and evaluate the thermodynamic parameters associated to the melting point of the compound. Fig. 6 shows the DSC curve for DMABA in solid state. The DSC scan clearly shows an endothermic peak located at 72.34 °C. This transition is attributed to the melting point of the sample. The estimated ΔH and ΔS variations for the phase transition are 19.21 kJ mol^{-1} and 55.61 J mol^{-1} K^{-1}, respectively. The broad peak located at 193 °C can be attributed to the decomposition of the substance.

Conclusions

A complete structural, thermodynamic, vibrational and electronic investigation along with FTIR, Raman, NBO analysis and

Please cite this article in press as: M. Rocha et al., Ab-initio and DFT calculations on molecular structure, NBO, HOMO–LUMO study and a new vibrational analysis of 4-(Dimethylamino) Benzaldehyde, Spectrochimica Acta Part A: Molecular and Biomolecular Spectroscopy (2014), http://dx.doi.org/10.1016/j.saa.2014.09.077

AIM approach of 4-(Dimethylamino) Benzaldehyde (DMABA) have been carried out with MP2 and DFT (B3LYP, mPW1PW91) methods using 6-31G(d,p) basis sets. The experimental IR and Raman spectra have been recorded and completely analyzed. The molecular geometry parameters, bond lengths and bond angles calculated with different methods and basis sets agreed well with the experimental values reported previously through X-ray diffraction methods. According to the RMSD values, the MP2 method reproduces better the experimental structure than other DFT methods; however the bond angles have a good correlation using the B3LYP method. A comparison of the results of experimental and theoretical study gave a full description of the vibrational properties of the title molecule. The TD-DFT calculation assisted the assignment of electronic transitions observed in the UV–visible absorption spectrum. The HOMO–LUMO energy gap is calculated to be 4.314 eV. This value explains the eventual charge transfer interaction with the molecule, which influences the biological activity of the compound. The relatively high value of $\Delta E_{\mathrm{HOMO-LUMO}}$ indicates that the title compound presents high chemical stability and it has low reactivity. DSC measurements show that the substance melts at 72.34 °C and decomposes at temperatures higher than 193 °C.

Acknowledgments

Authors thank CIUNT and CONICET (PIP 0205) for financial support. D.M.G. and J.M.A. thank CONICET for fellowships. A.D.S. thanks CIUNT for a fellowship.

Appendix A. Supplementary material

Supplementary data associated with this article can be found, in the online version, at http://dx.doi.org/10.1016/j.saa.2014.09.077.

References

[1] Y.X. Wu, J.H. Zhou, Yunnan Chem. Technol. 32 (2005) 20.
[2] L.H. Chernoff, Ind. Eng. Chem. Anal. Ed. 12 (1940) 273.
[3] G.W. Watt, J.D. Chrisp, Anal. Chem. 24 (1952) 2006.
[4] P. Pibarot, S. Pilard, Am. J. Anal. Chem. 3 (2012) 613.
[5] J.S. Esteve-Romero, Ll. Monferrer Pons, M.C. García-Alvarez-Coque, G. Ramis-Ramos, Anal. Lett. 27 (1994) 1557.
[6] P. Fritz, W. Van Bronswijk, S. Lewis, Analyt. Method 5 (2013) 3207.
[7] R. Callender, D. Chen, J. Lugtenburg, C. Martin, K.W. Rhee, D. Sloan, R. Vandersteen, K.T. Yue, Biochemistry 27 (1988) 3672.
[8] J.G. Rosencrance, P.W. Jagodzinski, Spectrochim. Acta A 42 (1986) 869.
[9] G.P. Kushto, P.W. Jagodzinski, Spectrochim. Acta A 54 (1998) 799.
[10] P.J.A. Ribeiro-Claro, P.D. Vaz, M. Nolasco, J. Mol. Struct. Theochem. 946 (2010) 65.
[11] M.J. Frisch, J.A. Pople, J.S. Binkley, J. Chem. Phys. 80 (1984) 3265. M.J. Frisch, G.W. Trucks, H.B. Schlegel, G.E. Scuseria, M.A. Robb, J.R. Cheeseman, J.A. Montgomery Jr., T. Vreven, K.N. Kudin, J.C. Burant, J.M. Millam, S.S. Iyengar, J. Tomasi, V. Barone, B. Mennucci, M. Cossi, G. Scalmani, N. Rega, G.A. Petersson, H. Nakatsuji, M. Hada, M. Ehara, K. Toyota, R. Fukuda, J. Hasegawa, M. Ishida, T. Nakajima, Y. Honda, O. Kitao, H. Nakai, M. Klene, X. Li, J.E. Knox, H.P. Hratchian, J.B. Cross, C. Adamo, J. Jaramillo, R. Gomperts, R.E. Stratmann, O. Yazyev, A.J. Austin, R. Cammi, C. Pomelli, J.W. Ochterski, P.Y. Ayala, K. Morokuma, G.A. Voth, P. Salvador, J.J. Dannenberg, V.G. Zakrzewski, S. Dapprich, A.D. Daniels, M.C. Strain, O. Farkas, D.K. Malick, A.D. Rabuck, K. Raghavachari, J.B. Foresman, J.V. Ortiz, Q. Cui, A.G. Baboul, S. Clifford, J. Cioslowski, B.B. Stefanov, G. Liu, A. Liashenko, P. Piskorz, I. Komaromi, R.L. Martin, D.J. Fox, T. Keith, M.A. Al-Laham, C.Y. Peng, A. Nanayakkara, M. Challacombe, P.M.W. Gill, B. Johnson, W. Chen, M.W. Wong, C. González, J.A. Pople, Gaussian 03, revision C.02, Gaussian Inc., Wallingford, CT, 2004.
[12] C. Møller, M.S. Plesset, Phys. Rev. 46 (1934) 618.
[13] A.D. Becke, J. Chem. Phys. 98 (1993) 5648.
[14] C. Lee, W. Yang, R.G. Parr, Phys. Rev. B 37 (1988) 785.
[15] C. Alamo, B. Barone, J. Chem. Phys. 108 (1998) 664.
[16] M.J. Frisch, A.B. Nielsm, A.J. Holder, Gaussview User Manual, Gaussian, Pittsburgh, 2008.
[17] V. Krishnakumar, G. Keresztury, T. Sundius, R. Ramanamy, J. Mol. Struct. 702 (2004) 9.
[18] E.D. Glendening, J.K. Badenhoop, A.D. Reed, J.E. Carpenter, F.F. Weinhold, Theoretical Chemistry Institute, University of Wisconsin, Madison, WI, 1996.
[19] R.F.W. Bader, Atoms in Molecules, A Quantum Theory, Claderon Press, Oxford, 1990.
[20] F. Biegler-Köning, J. Schönnbohn, D. Bayles, J. Comput. Chem. 22 (2001) 545.
[21] B. Gao, J.L. Zhu, Acta Cryst. E 64 (2008) 1182.
[22] V. Arjunan, L. Devi, R. Subbalakshmi, T. Rani, S. Mohan, Spectrochim. Acta A 130 (2014) 164.
[23] O.A. El-Gammal, T.H. Rakha, H.M. Metwally, G.M. Abu El-Reash, Spectrochim. Acta A 127 (2014) 144.
[24] T.A. Koopsmans, Physica 1 (1993) 104.
[25] R.J. Parr, L.V. Szentpaly, S. Liu, J. Am. Chem. Soc. 121 (1999) 1922.
[26] E. Scrocco, J. Tomasi, Adv. Quantum Chem. 11 (1979) 115.
[27] F.J. Luque, J.M. Lopez, M. Orozco, Theor. Chem. Acc. 103 (2000) 343.
[28] H. Kobinyi, G. Folkers, Y.C. Martin, 3D QSAR in Drug Design, Recent Advances, vol. 3, Kluwer Academic Publishers, 1998.
[29] S. Moro, M. Bacilieri, C. Ferrari, G. Spalutto, Curr. Drug Discov. Technol. 2 (2005) 13.
[30] N. Sundaraganesan, G. Mariappan, S. Manoharan, Spectrochim. Acta A 87 (2011) 67.
[31] E. Lizarraga, D.M. Gil, G.A. Echeverría, O.E. Piro, C.A.N. Catalán, A. Ben Altabef, Spectrochim. Acta A 127 (2014) 74.
[32] V. Arjunan, M. Kalaivani, S. Senthikumari, S. Mohan, Spectrochim. Acta A 115 (2013) 154.
[33] L.P. Avendaño Jiménez, G.A. Echeverría, O.E. Piro, S.E. Ulic, J.L. Jios, J. Phys. Chem. A 117 (2013) 2169.
[34] C. Sridevi, G. Shanthi, G. Velraj, Spectrochim. Acta A 89 (2012) 46.
[35] T.S. Xavier, I. Huber Joe, M.A. Palafox, S. Kumar, V.K. Rastogi, Spectrochim. Acta A 114 (2013) 502.
[36] M. Kumru, V. Küçük, M. Kocademir, Spectrochim. Acta A 96 (2012) 242.
[37] D. Lin-Vien, N.B. Colthup, W.G. Fateley, J.G. Grasselli, The Handbook of Infrared and Raman Characteristic Frequencies of Organic Molecules, Academic Press, 1991.